Magnetic Resonance in Medicine 52:704–708 (2004)

SSFP-Based MR Thermometry

Vaishali Paliwal,[1] AbdEl-Monem El-Sharkawy,[2] Xiangying Du,[3] Xiaoming Yang,[3] and Ergin Atalar[1–4]*

Of the various techniques employed to quantify temperature changes by MR, proton resonance frequency (PRF) shift-based phase-difference imaging (PDI) is the most accurate and widely used. However, PDI is associated with various artifacts. Motivated by these limitations, we developed a new method to monitor temperature changes by MRI using the balanced steady-state free precession (balanced-SSFP) pulse sequence. Magnitude images obtained with the SSFP pulse sequence were used to find the PRF shift, which is proportional to temperature change. Spatiotemporal temperature maps were successfully reconstructed with this technique in gel phantom experiments and a rabbit model. The results show that the balanced-SSFP-based method is a promising new technique for monitoring temperature. Magn Reson Med 52:704–708, 2004.

Key words: Key words: SSFP; proton resonance frequency shift; MRI; thermal mapping; ablation; MR thermometry

MR thermometry has recently gained attention for MR-based temperature mapping during the application of thermal therapies (1–3). When administering thermal therapies, it is important to ensure that the required thermal dose is delivered to the entire target tissue, and the surrounding important structures are spared thermal damage. MR thermometry can provide useful information for this purpose, since thermal maps can be constructed for the entire region of interest (ROI), and temperature variations of each pixel on the image can be monitored. This real-time feedback can be used by physicians administering thermal therapy to ensure successful treatment of the target tissue.

Many different temperature-monitoring techniques have been investigated to explore the possibility of using thermal mapping under MR guidance. Some of these techniques are based on measuring MR parameters, such as the T_1 relaxation time (4), diffusion coefficient of water (5), or proton resonance frequency (PRF) shift (6–8), which change along with temperature change. Different problems are associated with each of these techniques. Some of the most common problems relate to the accuracy of the temperature measurement, the repeatability of the experiments, difficulties in the calibration procedures, and the dependence of a method on geometry and orientation (6). These unsolved problems in MR thermometry techniques motivated us to find an alternative technique to measure the PRF shift.

A new balanced steady-state free precession (balanced-SSFP) based PRF shift temperature mapping technique is proposed in this paper. A similar principle has been used for blood oxygen level-dependent (BOLD) functional imaging (9,10). We demonstrate that the balanced-SSFP-based technique can be successfully used for both ex vivo and in vivo conditions.

THEORY

It is known that the balanced-SSFP pulse sequence is very sensitive to resonance frequency offsets (11,12). Magnitude images from a balanced-SSFP pulse sequence frequently show on- and off-resonance bands due to the inhomogeneity of the field.

The equation for the offset resonance angle, β_{total}, during steady-state magnetization is given by

$$\beta_{total} = \gamma \Delta B \, TR + \gamma r \cdot \int_0^{TR} G(t)dt + \omega_{cs} TR + \beta_{RF}, \quad [1]$$

where ω_{cs} is the frequency offset due to chemical shift, γ is the gyromagnetic ratio, r is the position vector, TR is the repetition time, ΔB represents the magnetic field inhomogeneity, and $G(t)$ is a time-varying gradient vector. β_{RF} is the phase difference between consecutive RF pulses, which can be controlled by the pulse sequence. The equation shows that the total offset resonance angle depends on four terms in the equation: the static field inhomogeneity, the gradient field inhomogeneity, the chemical shift, and the phase offset between consecutive RF pulses.

In the case of a balanced-SSFP pulse sequence, the integral of the gradient waveform over each repetition period is zero (12). Therefore, the equation for the offset resonance angle, β_{total}, during steady-state magnetization for balanced SSFP becomes:

$$\beta_{total} = \gamma \Delta B \, TR + \omega_{cs} TR + \beta_{RF}. \quad [2]$$

The signal intensity of a balanced-SSFP acquisition is a strong function of β_{total}. In balanced SSFP, the effects of β_{total} on the signal intensity can be seen when β_{RF} is varied in the pulse sequence by the addition of phase offsets between consecutive RF pulses. A plot of the signal intensity variations as a function of β_{total}, induced by β_{RF} changes, can then be obtained. These cyclic curves for which the signal intensity is plotted against the resonance

[1]Department of Biomedical Engineering, Johns Hopkins University, Baltimore, Maryland.

[2]Department of Electrical and Computer Engineering, Johns Hopkins University, Baltimore, Maryland.

[3]Department of Radiology, Johns Hopkins University School of Medicine, Baltimore, Maryland.

[4]Department of Electrical and Electronics Engineering, Bilkent University, Ankara, Turkey.

Grant sponsor: NIH; Grant numbers: RO1RR15396; R01HL61672; R01HL5748; Grant sponsor: NSF Engineering Research Center.

*Correspondence to: Ergin Atalar, Ph.D., Department of Radiology, Johns Hopkins University SOM, 720 Rutland Ave., Traylor Bldg., Rm. 330, Baltimore, MD 21205. E-mail: eatalar@mri.jhu.edu

Received 15 September 2003; revised 11 May 2004; accepted 11 May 2004.

DOI 10.1002/mrm.20231

Published online in Wiley InterScience (www.interscience.wiley.com).

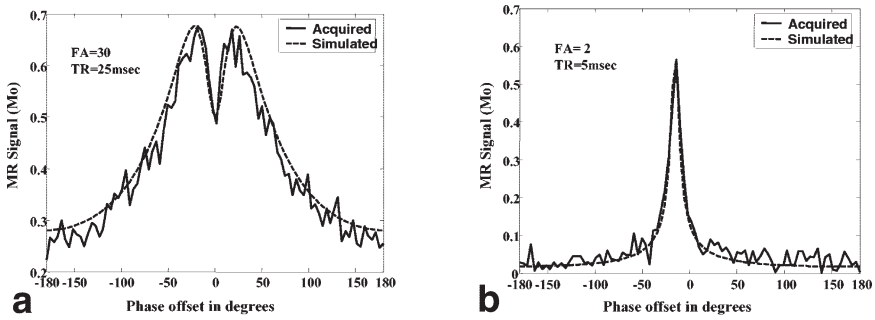

FIG. 1. Simulated and experimental frequency-offset curves for two cases: (**a**) high-FA/long-TR. FA of 30° and a TR of 25 ms were used. (**b**) low-FA/short-TR. An FA of 2° and a TR of 5 ms were used. In both cases, T_1 and T_2 were assumed to be 130/85 ms, respectively. Experimentally obtained data are overlaid with the simulated curve.

frequency offset are henceforth referred to as frequency-offset curves. In each frequency-offset curve there is a local minima or maxima when β_{total} is 0 or π. Figure 1a and b show simulated and experimentally obtained frequency-offset curves for high-flip-angle (FA)/long-TR and low-FA/short-TR cases, respectively. As shown in the figure, there is a good correlation between the simulated and experimentally obtained frequency-offset curves for both cases. The standard deviation (SD) is 3.3% and 2.8% of full magnetization, respectively.

It is known that the resonant offset frequency of water changes proportionally with temperature, introducing a change in the chemical shift offset, ω_{cs} (13)

$$\omega_{cs} = \alpha \Delta T \omega_0, \qquad [3]$$

where $\Delta\omega_{cs}$ is the change in chemical shift offset due to temperature changes, α is the proton resonance shift coefficient expressed in ppm/°C, ΔT is the temperature change, and ω_0 is the Larmor frequency. As shown in Eqs. [2] and [3], a balanced-SSFP pulse sequence can be used to calculate the PRF shift of water, which is proportional to the temperature change.

This new technique is based on the principle that if two frequency-offset curves as a function of β_{RF} obtained at different temperatures are correlated, there will be a phase shift between them due to the resonant frequency shift in water proportional to the change in temperature, as explained above.

The shape of the frequency-offset curve is a function of T_1, T_2, and FA. However, the local minima or maxima for each curve (when β_{total} is 0 or π) are not affected by T_1 changes, since they are a function of temperature only. As shown in Fig. 1a and b, both the high-FA/long-TR and the low-FA/short-TR cases result in curves with sharp maxima/minima peaks, and thus are suitable for the correlation technique. For both cases, we see that there is a local maxima/minima for each curve, and the position of this local minima/maxima remains constant even though the shape of the curves changes for different FAs and for changing T_1 values.

The actual implementation of the above temperature-monitoring technique using the balanced-SSFP pulse sequence is discussed below.

MATERIALS AND METHODS

We modified the balanced-SSFP pulse sequence to obtain the balanced-SSFP frequency-offset curve in real time during temperature changes. We obtained a group of images with various β_{RF} values to sample the balanced-SSFP frequency-offset curve, and repeated the scan several times in order to detect changes in the curve with temperature.

The software for postprocessing the data was developed with the use of Matlab software (Mathworks, Inc., Natick, Ma). Processing was done on each pixel for construction of a thermal map. The number of samples on each of these curves increased with the use of the cubic spline interpolation technique. Since the cubic spline interpolation technique gave satisfactory results, other (possibly more accurate) interpolation techniques, such as parametric curve fitting, were not analyzed. The amount of shift was estimated by means of a circular cross-correlation technique. The steps involved in processing each pixel are shown in Fig. 2. Samples for each frequency-offset curve are shown in graphs a and b. The original samples were then interpolated to give frequency-offset curves (Fig. 2c and d). Graph e shows the frequency offset curves in c and d superimposed. With the use of the cross-correlation technique, the amount of shift can be estimated, as shown in graph f.

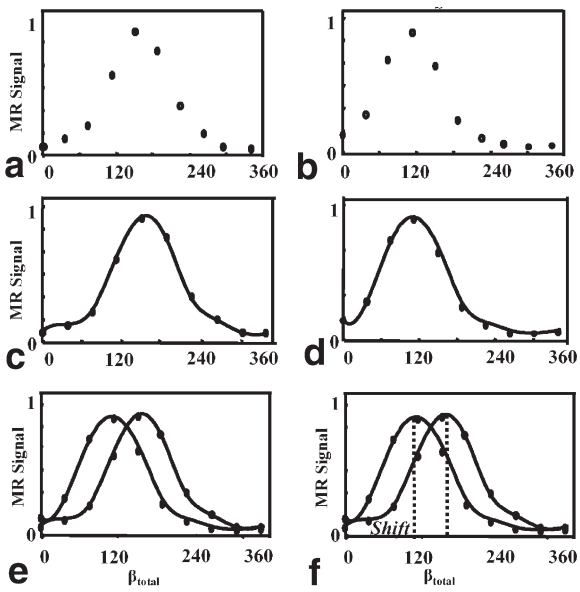

FIG. 2. Processing steps. **a** and **b:** Samples of frequency-offset curves acquired at different temperatures using a modified SSFP sequence. **c** and **d:** Interpolated frequency-offset curves obtained with a spline interpolation. **e** and **f:** Phase shift between two frequency-offset curves obtained at different temperatures. We can see phase shift between the peaks of the curves.

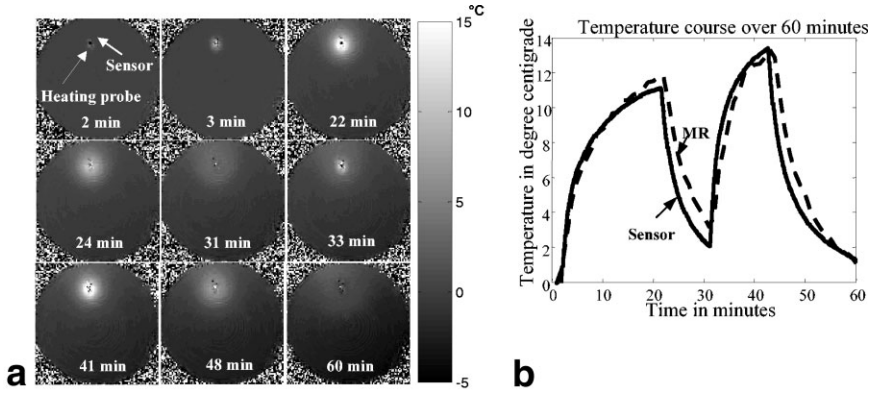

FIG. 3. Results of localized heating in a gel phantom using a microwave generator at 2.45 GHz. **a:** The temperature differences mapped during the course of the experiment are shown. Thermal maps are not reference-corrected, and the drift appears as the cooled region in the gel. **b:** Fiber-optic temperature probe and MR temperature measurements overlaid, as measured during the course of the experiment. For temperature comparison with fiber-optic temperature probe measurements, the MR temperature measurements shown on the graph are reference-corrected. For reference correction, the average drift was calculated using the region in the gel that was constant in temperature, and this drift was then subtracted from the entire image for drift correction.

The shift obtained from the correlation of frequency-offset curves at different temperatures was then converted to temperature change with the use of Eq. [3]. The PRF shift constant (α) that converts phase change to temperature change was assumed to be 0.01 ppm/°C, as stated in the literature (3,13).

A phantom experiment was designed to test the high-FA/long-TR case, and a rabbit experiment was designed to verify the low-FA/low-TR case.

EXPERIMENTS AND RESULTS

Microwave Heating Validation Experiment

A validation experiment was performed to determine the accuracy of the temperature measurements. A GdDTPA phantom with T_1/T_2 values of 130/85 ms was used for this experiment. A microwave generator operating at 2.45 GHz was used to localize heating of the gel phantom. A heating needle was inserted into the gel phantom, and a fiber-optic sensor was placed close to the heating needle to measure the temperature independently. For this purpose, a modified balanced-SSFP sequence was used on a GE 1.5 T Signa system with TR/TE = 25/1.4 ms, matrix = 256 × 192, FOV = 40 cm, and FA = 30°. A cylindrical phantom (diameter = 14 cm, height = 10 cm) was used. The microwave power was kept between 20–40 W. The axial plane was chosen for imaging. Twelve samples over each frequency-offset curve were obtained with the use of a high FA and TR. These 12 samples were acquired in approximately 1 min, and thus the temperature resolution was one sample per minute. We were able to increase the temporal resolution by decreasing the number of samples used to sample the frequency-offset curve. During the course of the experiment, the microwave was turned on for about 20 min, turned off for 10 min, turned on again for 15 min, and then turned off again. The experiment lasted for 60 min. We created thermal maps to map the temperature variations, and compared the temperature (measured by fiber-optic probe) with the temperature measurements obtained by MR to test the accuracy of this technique. To ensure that there was no temperature gradient between the gel phantom and the MR room itself, the phantom was left overnight in the scanner room before the experiment so that its temperature would stabilize.

The heating/cooling trend induced by the microwave generator is demonstrated by the fiber-optic measurements shown in Fig. 3b. Figure 3a shows a thermal map created during the course of the experiment. The graph in Fig. 3b shows an independent temperature measurement graph overlaid with temperature measurements from MR measurements averaged over 8 pixels near the fiber-optic probe. We used high-resolution images taken before the start of the heating experiment to locate the position of the fiber-optic probe. To compare MR measurements with independent optical temperature measurements, one must correct the MR temperature measurements for phase drifts. Since the experiment lasted about an hour, variations in baseline drifts were observed that required correction. We performed a reference correction for the temperature graph shown in Fig. 3b using a reference temperature calculated by averaging 5 × 5 pixels in the region of the gel that did not undergo temperature change. The temperature maps shown in Fig. 3a are not reference-corrected. Since microwave heat was used for this experiment, the heating was local and the temperature in the part of the gel away from the heating probe did not change. The number below each image represents the time point in the experiment that corresponds to the *x*-axis in the graph (given in minutes). The thermal maps show that the MRI measurement accurately followed the heating/cooling pattern produced by the microwave generator. The SD in the measurement between the fiber-optic temperature and MR temperature was calculated to be 1.2°C. The graph also shows that the MR temperature measurements followed the fiber-optic temperature variations accurately.

In Vivo Experiment in a Rabbit Model

An in vivo heating experiment was performed with the use of a rabbit model and a Signa 1.5 T scanner. The rabbit was

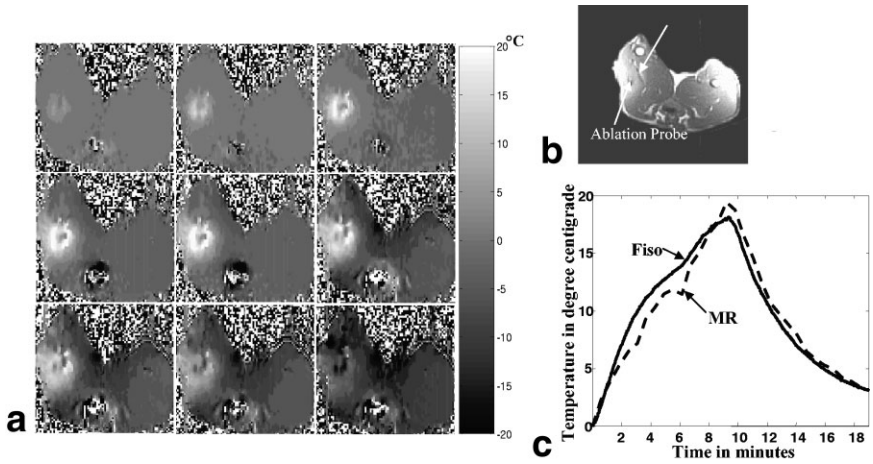

FIG. 4. Results of the in vivo rabbit experiment. **a:** Temperature difference maps during the course of the in vivo experiment. The temperature maps show heating during the time the microwave was switched on, and cooling after the microwave was switched off. **b:** Magnitude image of a rabbit thigh obtained with the use of a spin-echo pulse sequence. The positions of the fiber-optic sensor and the ablation probe are indicated on the image. **c:** Fiber-optic temperature measurement overlaid with the MR temperature measurements.

placed supine in the scanner, and a 3-inch dual surface coil was used in a phased-array configuration for imaging. Two MR-compatible biopsy needles were used to percutaneously puncture the right thigh of the anesthetized rabbit. A semi-rigid coaxial wire with an exposed whip was used as an ablation probe. The wire was inserted into the needle, and the needle was withdrawn after the ablation probe was positioned. Similarly, a fiber-optic temperature probe (FISO Technologies Inc., Quebec, Canada) was positioned through the second needle, which was placed close to the first needle. Thermal power was delivered from a microwave generator (Opthos Instruments, MD), positioned outside the scanner room and operating at 2.45 GHz, via coaxial cables running through a patch panel. The imaging slice was selected to include the sensitive region of the temperature sensor so that temperature measurements from the sensor could be compared with MR temperature measurements.

Two additional fiber-optic temperature probes were placed in the room to ensure that there was no temperature change in the scanner room. During ablation, balanced-SSFP-based PRF measurements were performed with the use of a modified balanced-SSFP sequence. The imaging parameters were TR/TE = 5/1.4 ms, FA = 2, FOV = 40, slice thickness = 10.3 mm, and matrix = 256 × 96. Sixty samples were acquired over each frequency-offset curve obtained using a low FA and TR. These also gave sharp peaks for frequency-offset curves for better correlation. As described above, a PRF-shift thermal coefficient of −0.01 ppm/°C was used to convert the phase shifts to temperature measurements. The microwave was turned on to deliver 40 W of power, which was later increased to 50 W. The microwave was turned off after about 10 min, and imaging was continued for another 10 min to record the cooling of the tissue. The experiment continued for 19 min, and 32 time points were obtained over that time.

Thermal maps of the rabbit thigh were created to visualize the extent of ablation. The fiber-optic temperature probe measurement was compared with the MR temperature measurements. Figure 4b shows the spin-echo image of the rabbit thigh, and the position of the ablation probe and the fiber-optic temperature sensor. This high-resolution image was used to locate the position of the fiber-optic sensor. The MR temperature was then compared with the temperature averaged over 25 pixels around the fiber-optic sensor. The maps obtained during the course of the experiment are displayed in Fig. 4a. Figure 4c shows the temperature measurement obtained with MRI overlaid over the fiber-optic temperature sensor measurements. The temperature maps are not reference-corrected. The reference correction for the temperature graph shown in Fig. 4c was performed in the same manner as in the gel experiment.

We can see that temperature measured with MR is in good agreement with the fiber-optic probe temperature measurements. The SD in the measurement between the fiber-optic temperature and MR temperature was calculated to be 1.8°C. The thermal maps accurately follow the heating and cooling trend produced by the microwave.

DISCUSSION

The selection of imaging parameters depends on the experimental procedure employed, and must be optimized. Two important considerations for parameter selection are the shape of the curve for effective correlation of the curve, and the required temporal resolution.

Currently, the total time required to acquire each temperature point is the time taken to acquire a single balanced-SSFP image multiplied by the number of images/sampling points used to sample a single frequency-offset curve. In the future, one could reduce this time by just sampling around the peak of the curve. For the ROI, the frequencies around which we need to sample in order to capture the peak can be detected from the scout image obtained at the start of the experiment.

The FA, along with the T_1 and T_2 of the target tissue, changes the shape of the frequency-offset curves. Simulations show that the use of high-FA/high-TR curves or low-FA/low-TR curves results in sharp minima/maxima peaks for better correlation between curves. The results showed that lower FAs (in the range of 3–5) are best suited for these experiments due to the shape of the frequency-offset curves. In addition, the dependence of the curves on the T_1/T_2 of the phantom decreases at lower FAs.

The number of samples over each curve, and the TR used will affect the temporal resolution of this technique. FA and TR can vary the shape of the frequency-offset

curves, and thus must be optimized. A complete analysis for optimization of TR and FA has not yet been done, but we know that if the TR is too long, the steady-state effect of the sequence is lost, and no on/off resonance effects are visible on the image. In addition, if a short TR is used, smaller FAs are more effective.

This balanced-SSFP-based technique is introduced here as a new temperature-monitoring technique. Further studies are required to determine how it compares to existing temperature-monitoring techniques.

CONCLUSIONS

We developed a new technique for monitoring temperature, and successfully tested it on gel phantoms and in vivo. As shown by the results of the experiments, the temperatures measured with the use of this technique agree with independent temperature measurements. The thermal maps matched the induced temperature rise and fall very well, both ex vivo and in vivo. We believe that this balanced-SSFP-based MR thermometry technique may be used as an alternative to current MR thermometry techniques.

ACKNOWLEDGMENTS

The authors thank Manoj Saranathan (GE Medical Systems) for providing the balanced-SSFP pulse sequence, Dan Rettman (GE Medical Systems) for his comments, Bensheng Qiu for technical support during the in vivo experiment, and Mary McAllister for her editorial assistance.

REFERENCES

1. Quesson B, de Zwart JA, Moonen CT. Magnetic resonance temperature imaging for guidance of thermotherapy. J Magn Reson Imaging 2000; 12:525–533.
2. Kettenbach J, Silverman SG, Hata N, Kuroda K, Saiviroonporn P, Zientara GP, Morrison PR, Hushek SG, Black PM, Kikinis R, Jolesz FA. Monitoring and visualization techniques for MR-guided laser ablations in an open MR system. J Magn Reson Imaging 1998;8:933–943.
3. Chen JC, Moriarty JA, Derbyshire JA, Peters RD, Trachtenberg J, Bell SD, Doyle J, Arrelano R, Wright GA, Henkelman RM, Hinks RS, Lok SY, Toi A, Kucharczyk W. Prostate cancer: MR imaging and thermometry during microwave thermal ablation-initial experience. Radiology 2000; 214:290–297.
4. Matsumoto R, Mulkern RV, Hushek SG, Jolesz FA. Tissue temperature monitoring for thermal interventional therapy: comparison of T_1-weighted MR sequences. J Magn Reson Imaging 1994;4:65–70.
5. Le Bihan D, Delannoy J, Levin RL. Temperature mapping with MR imaging of molecular diffusion: application to hyperthermia. Radiology 1989;171:853–857.
6. Peters RD, Hinks RS, Henkelman RM. Heat-source orientation and geometry dependence in proton-resonance frequency shift magnetic resonance thermometry. Magn Reson Med 1999;41:909–918.
7. Peters RD, Henkelman RM. Proton-resonance frequency shift MR thermometry is affected by changes in the electrical conductivity of tissue. Magn Reson Med 2000;43:62–71.
8. Kuroda K, Oshio K, Chung AH, Hynynen K, Jolesz FA. Temperature mapping using the water proton chemical shift: a chemical shift selective phase mapping method. Magn Reson Med 1997;38:845–851.
9. Scheffler K, Seifritz E, Bilecen D, Venkatesan R, Hennig J, Deimling M, Haacke EM. Detection of BOLD changes by means of frequency-sensitive trueFISP technique: preliminary results. NMR Biomed 2001;14: 490–496.
10. Miller KL, Hargreaves BA, Lee J, Ress D, deCharms RC, Pauly JM. Functional brain imaging using blood oxygenation sensitive steady state. Magn Reson Med 2003;50:675–683.
11. Oppelt A, Graumann R, Barfuss H, Fischer H, Hartl W, Schajor W, et al. FISP—a new fast MRI sequence. Electromedica 1986;54:15–18.
12. Haacke RM, Brown RW, Thompson MR, Venkatesan R. Magnetic resonance imaging: physical principles and sequence design. New York: John Wiley & Sons; 1999.
13. Hindman JC. Proton resonance shift of water in the gas and liquid states. J Chem Physics 1966;44:4582–4592.